*Regular Article*

INORGANIC CHEMISTRY RESEARCH
Published by the
*Iranian Chemical Society*
www.inorgchemres.org
info@inorgchemres.org

***Inorg. Chem. Res.**, Vol. 5, No. 1, 94-111, June 2021*
**DOI: 10.22036/icr.2021.238089.1076**

# Theoretical Investigation of 4-Methyl-4H-1,2,4-triazole-3-thiol and Its Mononuclear and Dinuclear Palladium(II) Complexes; Molecular Structure, NBO Analysis, FT-IR and UV-Vis Spectroscopy

Sara Seyfi[a], Robabeh Alizadeh[a,*], Masoud Darvish Ganji[b,*] and Vahid Amani[c]

[a]*School of Chemistry, Damghan University, P. O. Box: 36715-364 Damghan, Iran*
[b]*Department of Chemistry, Islamic Azad University, Qaemshahr, Iran*
[c]*Department of Chemistry, Farhangian University, Tehran, Iran*

*(Received 5 July 2020, Accepted 13 January 2021)*

In this research, the characterization of complexes [Pd(aemptrz)$Cl_2$] (1), [$Pd_2$(μ-mptrz)$_2$(mptrz)$_2$(en)].$CH_3OH$ (2) [$Pd_2$(μ-mptrz)$_4$] (3) and [$Pd_2$(μ-mptrz)$_2$(mptrz)$_2$(en)] (4) (where aemptrz is 1-(1-($\lambda^2$-azanyl)ethyl)-4-methyl-5-($\lambda^1$-sulfanyl)-4H-1$\lambda^4$,2,4-triazole, en is ethylene diamine and Hmptrz is 4-methyl-4H-1,2,4-triazole-3-thiol) were carried out by Density Functional Theory (DFT) calculations. Structural, electronics and molecular properties (such as bond distances, bond angles, energies of highest occupied molecular orbital ($E_{HOMO}$), the lowest unoccupied molecular orbital ($E_{LUMO}$), the energy gap (ΔE), chemical hardness η, the dipole moment μ and Natural bond orbital (NBO) analysis of compounds) have been investigated using density functional theory at two different functional methods (B3LYP and M06). Moreover, electronic structures of all complexes via NBO calculation show that Pd-N and Pd-S bonds are made of delocalization of occupancies from lone pair (LP) orbital of N, S atoms to the palladium atom. The FT-IR spectroscopy analysis and electronic spectra were calculated using B3LYP/TZVP basis set and compared with the experimental values. Furthermore calculation of vibrational spectra are also allocated based on the potential energy distribution (PED) using the *VEDA 4* program. The electronic spectra were calculated using DFT and time dependent density functional theory (TD-DFT) methods.

**Keywords:** 4-Methyl-4H-1,2,4-triazole-3-thiol, Palladium(II) complexes, Energy gap, Chemical hardness η, Dipole moment μ, Density functional theory (DFT), Potential energy distribution (PED), TD-DFT

## INTRODUCTION

Despite the long history of heterocyclic chemistry, it has only recently been discussed as a separate branch [1]. The heterocyclic chemistry have found numerous applications in drug synthesis such as antibiotics [2-4], pesticides [5] and good correlated fields of material sciences [6], biochemistry [7] and dyes industry [8,9].

A possible phenomenon for the heterocyclic compounds is tautomerism, which results as the equilibrium between two or more structural isomers [10]. Knowing the stability of a tautomeric form in relation with other forms plays an important role in solving the ambiguities from a structural chemistry viewpoint. Tautomerism depends on several phenomena such as different types of migrating groups (electrophile or nucleophile) and migration of neutral groups. The 1,2,4-triazole derivatives (*e.g.* Hmptrz) are a 5-membered heterocyclic compound and have two tautomeric forms which are resulted from the replacement of hydrogen atom position. If the hydrogen atom binds to the nitrogen and sulfur, the thione and thiol forms will be created, respectively [11,12]. Moreover, hetero-aromatic

*Corresponding authors. E-mail: robabeh_alizadeh@yahoo.com; ganji_md@yahoo.com

chelates based on 1,2,4-triazole are among the crucial ligands for inorganic cations. Previous studies [13-15] have shown that if functional groups are attached to hetero-aromatic ring, this will affect the reactivity of the ring [16]. Accordingly, in this study first 4H-1,2,4-triazole-3-thiole molecule has been investigated without considering the functional group ($CH_3$). On the other hand, following evaluation of substitution of methyl on the aromatic ring and its effect on reactivity has also been studied.

On the other hand, in the past several years, researchers have focused on palladium complexes due to its biological [17,18] and catalytic activities [19,20], high solubility [21], structural and thermodynamic properties [22]. Palladium complexes with heterocyclic N,S-containing ligands, have shown good antitumor, antibacterial and anticancer activities [23]. The catalytic efficiency of palladium(II) complexes in numerous reactions such as carbon-carbon and carbon-nitrogen bond-forming reactions has also been extensively studied. Despite the large body of literature on the reactivity of palladium complexes, electronic structures of these complexes have been much less studied [24]. While most previous studies have focused on complexes containing N-heteroaromatic ligands and a number of metals including ruthenium(II), osmium(II) and rhenium(I), complexes with $d^8$ metals have received much less attention. For this reason, study of the electronic structures of such complexes is valuable for the prediction of their properties [25-27].

In this study, to prove and better understand the obtained experimental data, the calculations of density functional theory (DFT) have been used. In the theoretical section of this research, we first studied the details of tautomeric process of thione-thiol form of triazole and its derivatives. The geometry of ligand and its Pd(II) complexes were optimized and quantum chemical parameters have been investigated. In addition, through NBO analysis, we dealt with the tendency of the donor-acceptor interactions between ligand and complexes. Spectroscopic examination of FT-IR has been done using DFT/B3LYP method TZVP basis set. The molecular structure of the triazole and its derivatives and of [Pd(aemptrz)$Cl_2$] (1), $Pd_2(\mu\text{-mptrz})_2(mptrz)_2(en)].CH_3OH$ (2) [$Pd_2(\mu\text{-mptrz})_4$] (3) and [$Pd_2(\mu\text{-mptrz})_2(mptrz)_2(en)$] (4) [28] have been shown in Figs. 1-3.

## COMPUTATIONAL DETAILS

All calculations were performed using density functional theory (DFT) with ORCA (version 3.03) program package [29]. The DFT calculations used the hybrid B3LYP density functional (Becke's three parameter nonlocal exchange functional along with the Lee-Yang-Parr correlation functional [30,31]. In all the calculations, we employed the new efficient RIJCosX algorithm [32,33] and the recent Grimme semi-empirical atom pair-wise correction (D3)-commonly known as DFT-D3- to calculate the dispersion constant in van der Waals interactions. We utilized the [SD (28, MDF)] effective core potential (ECP) for the Pd atom [34,35]. Furthermore, the population analysis was carried out using the natural bond orbital (NBO) method [36]. In this paper, we report a comparative study of natural bond orbital by two different functional methods, B3LYP and MO6 [37]. Dipole moments are obtained with the B3LYP method. Solvent effects were included in calculation of complex 2 using a COSMO [38] implicit solvation model appropriate for methanol.

The electronic transitions between HOMO and LUMO were calculated at Restricted Kohn-Sham (RKS) and TD-DFT/B3LYP TZVP level of theory, with 50 singlet excited states that result in the UV-Vis spectra and the main orbitals contributing to the transitions. The optimized ground state configurations of title compounds were used as starting configurations for the TD-DFT calculations. TD-DFT calculations were performed with no symmetry constraints [39].

The molecular structure of the triazole and its derivatives and of 1-4 complexes were optimized by DFT-B3LYP method. The vibrational spectra (IR), quantum chemical parameters (such as $E_{HOMO}$, $E_{LUMO}$, energy gap, chemical hardness $\eta$ and dipole moment ($\mu$)) were also calculated with these methods. The calculated vibrational frequencies were also allocated *via* potential energy distribution (PED) analysis of all the fundamental vibration modes by the use of the VEDA 4 program [40,41]. All the vibrational assignments were based on the B3LYP/TZVP level calculations.

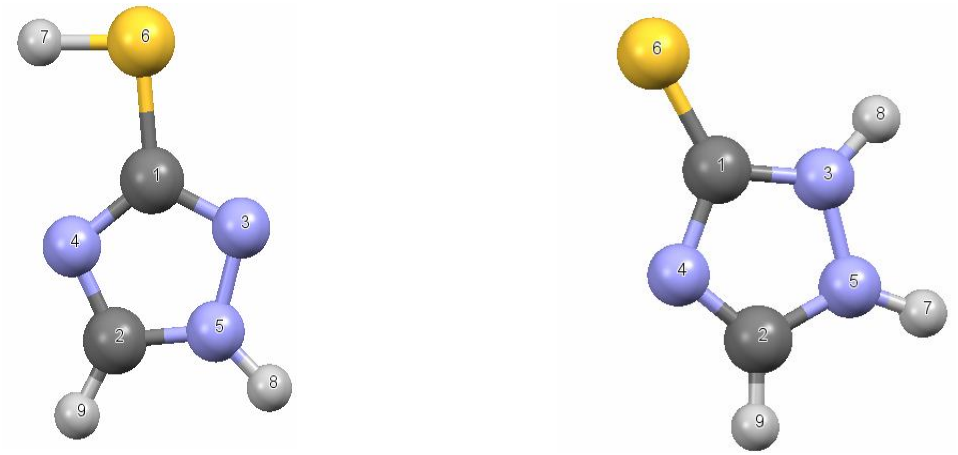


**Fig. 1.** Tautomeric (thiol, thione) forms of triazole derivatives with numbering of atoms.

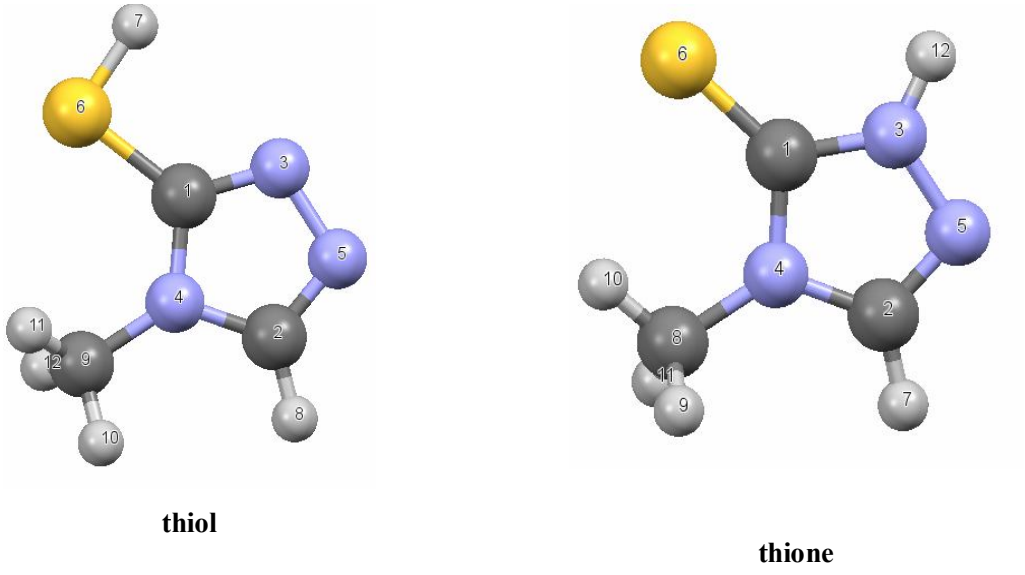


**Fig. 2.** Tautomeric (thiol, thione) forms of Hmptrz along with numbering of atoms.

## RESULTS AND DISCUSSION

### Molecular Geometry

We performed the DFT calculations of 4H-1,2,4-triazole-3-thiol and its derivatives by B3LYP method with TZVP basis set. Figures 1 and 2 represent the molecular structure and atomic numbering of 4H-1,2,4-triazole-3-thiol and its derivatives. Table 1 shows a comparison between the optimized structures by B3LYP/6-311++G(d,p) [42]/TZVP and selected structural parameters by X-ray diffraction [43]. In the optimized structure of the triazole ring, the N-N, C-N bond lengths and the N-C-N, N-N-C bond angle are 1.365,

**Table 1.** Comparative Selected Bond's Lengths (Å) and Bond's Angles (°) for Hmptrz Experimental and Theoretical Calculations by DFT. B3LYP/B3LYP6-311++G(d,p)/TZVP

| Bond length | B3LYP6-311++G(d,p) Theoretical calculations reference [42] | B3LYP-TZVP | EXP [43] |
|---|---|---|---|
| C=S | 1.667 | 1.661 | 1.675 |
| N3-N5 | 1.382 | 1.365 | 1.379 |
| N3-H12 | 1.015 | 1.005 | 0.89 |
| C2-N4 | 1.369 | 1.360 | 1.326 |
| Bond angles | | | |
| S6-C1-N3 | 127.7 | 128.54 | 125.9 |
| N4-C1-N3 | 101.5 | 101.91 | 102.8 |
| N3-N5-C2 | 104.9 | 103.43 | 104.1 |

**Table 2.** Geometrical Parameters (Hmptrz) and 1,2,4-Triazole Ligands

| Bond lengths (Å) | Hmptrz (thiol) | Hmptrz (thione) | 1,2,4-Triazole (thiol) | 1,2,4-Triazole (thione) |
|---|---|---|---|---|
| S-H | 1.343 | - | 1.342 | - |
| C1-S | 1.757 | 1.661 | 1.757 | 1.652 |
| C1-N3 | 1.310 | 1.360 | 1.322 | 1.377 |
| N3-N5 | 1.360 | 1.365 | 1.357 | 1.374 |
| C2-N5 | 1.302 | 1.295 | 1.343 | 1.348 |
| C2-N4 | 1.370 | 1.365 | 1.317 | 1.301 |
| C1-N4 | 1.367 | 1.386 | 1.365 | 1.392 |
| Bond angles (°) | | | | |
| N3-C1-S6 | 126.76 | 128.54 | 121.17 | 124.32 |
| N3-C1-N4 | 110.87 | 101.91 | 115.03 | 106.11 |
| N4-C1-S6 | 128.22 | 129.56 | 123.80 | 129.57 |
| N4-C2-N5 | 110.89 | 112.29 | 110.04 | 112.98 |
| N5-C2-H8 | 126.08 | 124.24 | 123.75 | 121.25 |
| N4-C2-H8 | 123.03 | 123.46 | 126.21 | |
| C1-N4-C2 | 103.22 | 107.92 | 102.77 | 107.10 |
| C1-S6-H9 | 92.71 | - | 93.67 | - |

1.360 Å and 101.91, 103.43°, respectively which are in good agreement with reported theoretical parameters [42] and experimental values [43].

Selected bond lengths and angles are summarized in Table 2. The bond lengths of C1-N3 and C1-N4 in thione form is longer than thiol form, which can be due to increased participation of the *p* orbital of these bonds and thus decrease of the participation percentage of *s* orbital in the bonds. NBO analysis has shown that hybridization in thiol form is $sp^{1.51}$ (on nitrogen atom with a mixture of orbitals *s* (39.76%) *p* (60.18%) *d* (0.06%)) and in thione form is $sp^{1.61}$ (on nitrogen atom with a mixture of orbitals *s* (38.29%) *p* (61.55%) *d* (0.16%)) (Table S1).

The ascending trend of bond length and participation percentage of *p* orbital in carbon-nitrogen bonds in thione form in comparison with thiol form is due to elevation of the base properties of nitrogen lone pairs electrons in this form (Table S1). Furthermore, the decrease in the bond length of C1-S in thiol form suggests that the bond is double and sulfur is deprotonated (Table 2).

Investigation of the bond length between optimized structures to examine the role of the methyl functional group on the triazolyl ring has indicated that the bond length of C2-N4 is longer in structures in which methyl group is present on the ring. In response to the presence of the functional group $CH_3$, the length of this bond has shown a better correspondence with single bond (Table 2). As can be seen in the Table 2, N4-C1-S6 and N3-C1-N4 bond angles increase in thione form while this angles decrease in thiol form due to changes in hybridization from $sp^3$ to $sp^2$ (Table S1).

The optimized structure and numbering atoms of complexes 1-4 are shown in Fig. 3 and selected bond lengths and angles are reported in Table 3.

The bond lengths of Pd-N, Pd-S, S-C(6), N(14)-N(16) and C(6)-N(14) in the complex 1 were 2.033, 2.291, 1.682, 1.398 and 1.373 Å, respectively. Which are longer than those found for Hmptrz ligand this maybe due to increase, in the participation of *p* orbital and lack of participation of *s* orbital in these bonds (Table S2). Reported herein are the complexes with metal-metal ($d^8$-$d^8$) interaction, which are supported by bridging ligand (complex 2, 3) and/or absent bridging ligand (complex 4) [44]. The previous study [45] of the Pd-Pd bonds indicated that mixing between the valence 5*pz*, 5*s*, $4dz^2$ orbitals is occurring. The Pd-Pd bond order for complexes 2, 3 and 4 are calculated by the DFT-B3LYP/TZVP method (Table 4). The Pd-Pd distances of the complexes 2, 3 and 4 are slightly longer than the experimental values (0.005, 0.0574 and 0.068 Å, respectively). Notably, for calculated Pd-Pd distance of 2.837 Å in complex 3, we suggest that the metal-metal interaction overcomes the columbic repulsion between the two dicationic Pd centers [44,45]. Moreover, this may indicate that more electrons were shared between the two Pd atoms [46].

The results given in Table 3 indicated that the optimized parameters by DFT-B3LYP/TZVP method are slightly longer than the experimental one, attributed to the fact that the experimental data are for the molecules in the solid state and the theoretical calculations were performed for an isolated molecule in the gas phase. It is evident that the geometry in the solid state structure was exposed to an intramolecular force such as π-π interactions and hydrogen bonding.

## HOMO, LUMO, Energy Gap and Dipole Moment

The calculated quantum chemical parameters, such as energy band gap, chemical potential, chemical hardness, dipole moment, electrophilicity and total energy presented in Table 5.

The aim of this study is to evaluate the activity and stability of triazole, its derivatives and the comparison of quantum chemical parameters after coordination of Hmptrz ligand to Pd atom using Eqs. (1) to (4) [47].

$$\text{Gap Energy} = E_{LUMO} - E_{HOMO} \quad (1)$$

Where $E_{HOMO}$ is the energy of the highest occupied molecular orbital and $E_{LUMO}$ is the energy of the lowest unoccupied molecular orbital.

In addition, hardness (η) can be calculated using the Koopmans' theorem [48]

$$\eta = (E_{Lumo} - E_{Homo})/2 \quad (2)$$

Chemical potential (μ) is defined based on the subsequent equation [48]

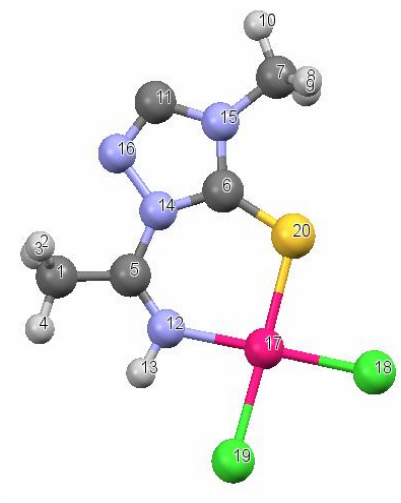

**Complex 1**

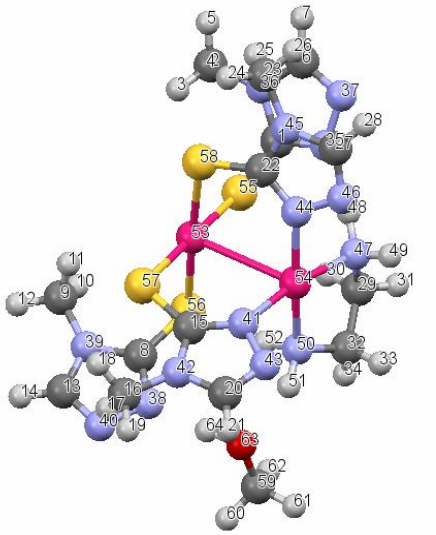

**Complex 2**

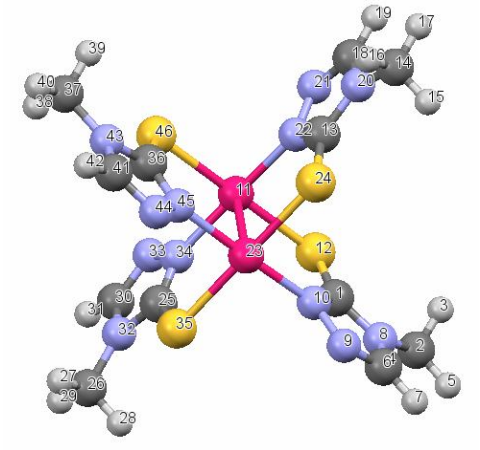

**Complex 3**

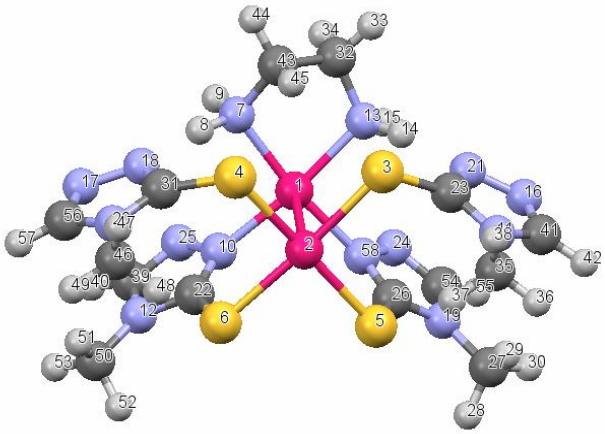

**Complex 4**

**Fig. 3.** The optimized structure of 1, 2, 3 and 4 complexes.

$$\mu = -(E_{Lumo} + E_{Homo})/2 \quad (3)$$

Electrophilicity (ω) [48] is described as the subsequent equation.

$$\omega = \frac{\mu^2}{\eta \times 2} \quad (4)$$

Comparison of $E_{HOMO}$ in previous studies indicates that [49-51] the high $E_{HOMO}$ values caused the molecule has a tendency to donor electrons to convenient acceptor with low energy vacant molecular orbital. Furthermore, the lower value of $E_{LUMO}$ enhances capacity of the molecules to accept electrons in electron transmission process [52].

Energy band gap ΔE is a crucial scale of stability and electrical transport properties since, it is a measure of electron conductivity [53]. The energy gap is the difference of energy value between HOMO and LUMO states. Comparison of the energy gap in complexes suggests that the low value of ΔE allows for better electron absorption

**Table 3.** Comparative Selected Bond Lengths (Å), Angles and Torsion Angles (°) of Complexes 1, 2, 3 and 4

| Bond lengths (Å) | DFT | EXP [28] | Bond angles (°) | DFT | EXP [28] |
|---|---|---|---|---|---|
| | | Complex 1 | | | |
| Pd17-S20 | 2.291 | 2.2436(12) | Cl18-Pd17-Cl19 | 93.65 | 92.85(4) |
| Pd17-N12 | 2.033 | 1.988(4) | S20-Pd17-N12 | 93.75 | 94.85(11) |
| Pd17-Cl18 | 2.295 | 2.3160(13) | Cl18-Pd17-S20 | 86.85 | 85.88(4) |
| Pd17-Cl19 | 2.317 | 2.3318(11) | Cl19-Pd17-N12 | 85.58 | 86.56(13) |
| C6-S20 | 1.682 | 1.676(4) | S20-C6-N15 | 124.27 | 124.3(3) |
| C6-N14 | 1.373 | 1.374 | | | |
| N14-N16 | 1.398 | 1.387 | | | |
| | | Complex 2 | | | |
| Pd54-Pd53 | 3.054978 | 3.0504(7) | S56-Pd5,-S55 | 82.47 | 82.55(6) |
| Pd53,S55 | 2.4019 | 2.3267(17) | S55-Pd53-S58 | 94.80 | 94.83(6) |
| Pd53-S56 | 2.4115 | 2.3362(17) | S57-Pd53-S58 | 88.84 | 87.22(6) |
| Pd53-S57 | 2.4115 | 2.3244(16) | S56-Pd53-S57 | 93.91 | 95.06(7) |
| Pd53-S58 | 2.4048 | 2.3296(17) | N50-Pd 54-Pd 53 | 94.18 | 100.19(12) |
| Pd54-N41 | 2.0299 | 2.043(4) | N47-Pd54-N50 | 83.43 | 83.48(18) |
| Pd54-,N44 | 2.0324 | 2.041(4) | N44-Pd54-N50 | 173.09 | 173.89(18) |
| Pd54-N47 | 2.0696 | 2.004(4) | N41-Pd54-N44 | 97.33 | 96.03(16) |
| Pd54-N50 | 2.0583 | 2.025(4) | N44-Pd54-N47 | 90.37 | 90.85(18) |
| O63-H64 | 1.0017 | 1.02(5) | N41-Pd54-N50 | 89.19 | 89.37(4) |
| | | | L(N38,H64,O63,H51,2) | 181.96 | 167(12)' |
| | | | L(N38,H64,O63,H51,1) | 178.22 | 154(12) |
| | | Complex 3 | | | |
| Pd23-Pd11 | 2.837 | 2.779(10) | S12-Pd11-N22 | 90.18 | 90.15(9) |
| Pd11-S12 | 2.394 | 2.3315(12) | N34-Pd11-S46 | 90.18 | 90.15(9) |
| Pd11-N22 | 2.032 | 2.068(3) | S24-Pd 23-N45 | 89.81 | 89.93(9) |
| Pd11-N34 | 2.023 | 2.068(3) | N10-Pd23-S35 | 89.80 | 89.93(9) |
| Pd11-S46 | 2.394 | 2.332(12) | Pd11-N34-N33 | 122.35 | 124.4(3) |
| Pd23-N10 | 2.023 | 2.068(3) | Pd11-Pd 23-S35 | 89.90 | 91.63(4) |
| Pd23-S24 | 2.394 | 2.332(12) | N10-Pd 23-Pd11 | 88.06 | 88.74(11) |
| Pd23-S35 | 2.394 | 2.332(12) | | | |
| Pd23-N45 | 2.034 | 2.068(3) | | | |

**Table 3.** Continue

| Complex 4 | | | | | |
|---|---|---|---|---|---|
| Pd1-Pd2 | 3.110 | 3.042 | N13-Pd1-N58 | 87.83 | 89.70 |
| S3-Pd2 | 2.395 | 2.341 | N7,Pd1,N13 | 83.63 | 83.59 |
| S4-Pd2 | 2.402 | 2.349 | N7-Pd1-N10 | 90.98 | 89.72 |
| S5-Pd2 | 2.408 | 2.336 | N10-Pd1-N58 | 97.56 | 96.99 |
| S6-Pd2 | 2.399 | 2.338 | S5,Pd2,S6 | 87.29 | 87.3 |
| N7-Pd1 | 2.057 | 2.006 | S4-Pd2-S6 | 93.44 | 93.97 |
| N10-Pd1 | 2.041 | 2.046 | S3-Pd2-S5 | 96.47 | 96.11 |
| N13-Pd1 | 2.066 | 2.001 | S3-Pd2-S4 | 82.88 | 81.82 |
| N58-Pd1 | 2.032 | 2.004 | | | |
| N18-N17 | 1.365 | 1.394 | | | |
| N25-N10 | 1.368 | 1.386 | | | |

**Table 4.** Mayer Bond Orders for the 2, 3 and 4 Complexes

| Bond order | 2 | 3 | 4 |
|---|---|---|---|
| Pd-Pd | 0.1326 | 0.2960 | 0.1393 |

**Table 5.** Calculated Total Energy, Orbital Energies $E_{HOMO}$ and $E_{LUMO}$, Gap Energy ΔE, Chemical Hardness η and Dipole Moment μ for 1,2,4-Triazole , its Derivatives (Hmptrz) Ligand and 1, 2, 3 and 4 Complexes

| Compound | $E_{HOMO}$ | $E_{LUMO}$ | Gap energy ΔE (eV) | Chemical hardness η (eV) | Dipole moment μ (Debeyes) μD | Electroplisity (ω) | Chemical dipole | Total energy |
|---|---|---|---|---|---|---|---|---|
| Hmptrz (thiol) | -6.485 | -0.255 | 6.229 | 3.114 | 5.134 | 1.823 | 3.370 | -679.663 |
| 1,2,4-Triazole (thione) | -5.488 | -1.133 | 4.354 | 2.177 | 8.198 | 2.517 | 3.311 | -640.351 |
| Hmptrz (thione) | -5.753 | -0.395 | 6.148 | 3.074 | 3.567 | 1.763 | 3.074 | -640.375 |
| 1,2,4-Triazole (thiol) | -6.595 | -1.214 | 5.381 | 2.690 | 3.139 | 2.833 | 3.905 | -679.686 |
| 1 | -6.709 | -2.865 | 3.843 | 1.921 | 4.259 | 5.962 | 4.787 | -1860.073 |
| 2 | -5.205 | -1.819 | 3.385 | 1.692 | 3.569 | 3.644 | 3.512 | -3276.485 |
| 3 | -5.054 | -1.448 | 3.606 | 1.803 | 0.004 | 2.931 | 3.251 | -2972.358 |
| 4 | -5.128 | -1.688 | 3.440 | 1.720 | 3.776 | 3.376 | 3.409 | -316.884 |

and bond flexibility with a metal atom, as the energy required for removing electron from the last occupied orbital (HOMO) will be low. Table 5 indicates that the 1,2,4-triazole (thiol) possess the greater value of HOMO energy ($E_{HOMO}$ = -6.595 eV) comparatively to the $E_{HOMO}$ of other molecules under investigation.

The obtained results from Table 5 indicate that the Hmptrz (thiol) displays the higher value of energy gap (ΔE = -6.299 eV) than that molecules under investigation as a hard molecule. Presumably, the Hmptrz presents a high kinetic stability, and chemical hardness, because it is energetically unfavorable to add electrons to a low-energy LUMO and to accept electrons from a high- energy HOMO [54].

The results given in Table 5 indicated that the higher value of energy gap index presents that the complex 1 is better electron acceptor than three complexes under investigation. Moreover, complex 2 had the lowest band gap compared to the other three complexes. This means that the complex showed a high reactivity with the appropriate donor site [52-54]. The data can be well applied to the further biochemistry studies.

In this study the energy gap ΔE of the complexes 1-4 indicated the following order

1 > 3 > 4 > 2

As can be observed, the energy gap for all complexes is smaller than the Hmptrz.

Chemical hardness parameter was used to evaluate the reactivity of the all complexes using Eq. (2) of Koopmans' theorem [48].

Study of the chemical hardness of the complexes 1-4 indicated the following order, *i.e.* the increase of the stability and decrease of reactivity occur

2 > 4 > 3 > 1

The results indicate that complex 2 shows a greater reactivity than the other three studied complexes (Table 5).

## Dipole Moment

A dipole moment is created by the lack of uniform charge distribution and shows the polarity of the molecules [55-56]. Moreover, it was observed that the value of the dipole moment is of the following order for triazole and its derivatives.

Hmptrz (thiol) > Triazole (thiol) > Hmptrz (thione) > Triazole (thione)

In the present work, complex 1 had a greater solubility in polar solvents:

1 > 4 > 2 > 3

On the other hand, most of the investigations of the dipole moment of the complex 2 were done in three ways: (a) evaluating the complex without a solvent in the crystal structure (b) evaluating the complex with a solvent in the crystal structure (c) evaluating the complex with dielectric constant of methanol solvent. We noted that the dipole moment of complex 2 was 3.437, 3.385 and 6.044 (De) for the calculations a, b and c, respectively. Dihedral angles of the complex 2 without considering methanol solvent, between the best planes of Pd53/S55/S56/S57/S58 and Pd54/N50/N47/N44/54/41 is 16.98°. However, the dihedral angle between these planes, when methanol is considered, changes to 14.35°. The reduction in the dihedral angle can be attributed to the existence of hydrogen bond due to the presence of methanol. In complex 2, methanol forms a N38…H64…O63 hydrogen bond. As can be seen in Fig. 4, indeed methanol also acts as donor through proton and as acceptor of the hydrogen bond through oxygen and nitrogen (of triazole ring). This bond plays an important role in structural stability. The calculated $O_{63}…H_{51}$ and N38…H64 bond distances in this complex are 1.881 Å and 1.726 Å respectively.

As can be seen in Table 5, the dipole moment of the complexes 1-4 is lower than the triazole and its derivatives. Indeed, it can be stated that after the formation of the complexes, the dipole moment of the complexes decreases. Several conclusions can be made from quantum chemical parameters:

I) The energy gap and chemical hardness are directly related, *i.e.*

II) The trend of changes in chemical potential was reported, which was congruent with the result obtained from energy gap and chemical hardness. This is because the more negative the chemical potential, the more heat is produced by the reaction, thus showing more reactivity.

## Frontier Molecular Orbitals

The reason of investigating the frontier orbitals of the Hmptrz ligand and synthesized complexes is to answer this question that "how the energy level of these orbitals change

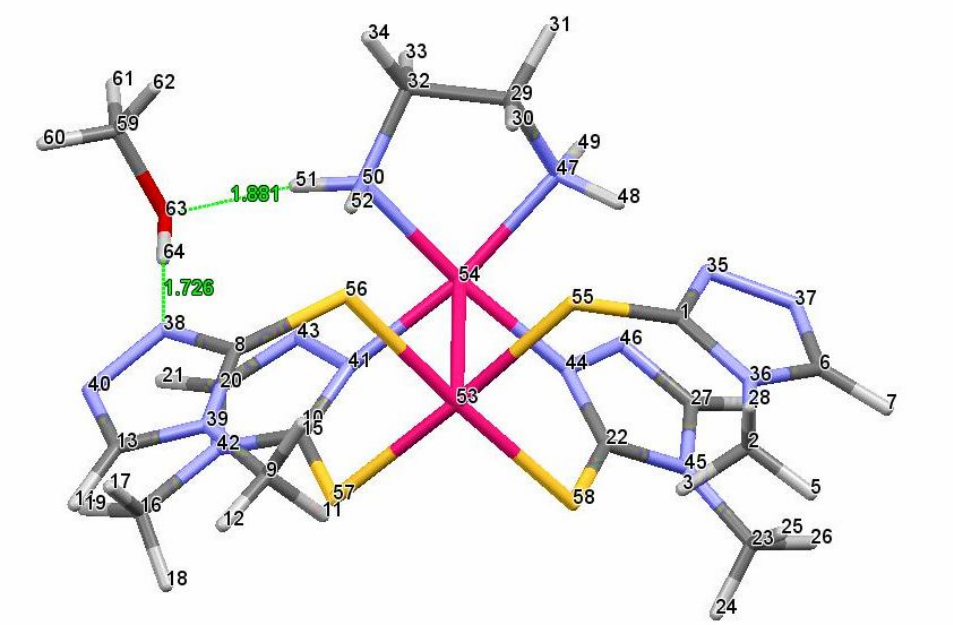


**Fig. 4.** Hydrogen bonds O-H••• N of complex 2.

following the entrance of the ligand in to the complex?" Further, the reactivity of the molecule depends on the distribution of electron cloud in their molecular orbitals. In this regard, the Frontier orbitals of the synthesized complexes have been examined. Figure S1 shows (HOMO-2, HOMO-1, HOMO, LUMO, LUMO+1 and LUMO+2) states with B3LYP/TZVP method. As can be seen in the figure S2, in investigation of the HOMO and LUMO of the Hmptrz ligand, as a comparison it can be stated that the density of the electron cloud exists throughout the entire space of the two central orbitals of this molecule. This can be attributed to the distribution of π electron cloud in this molecule. HOMO density is close to the region of triazole ring and thiol group, which can be due to the pair electrons of nitrogen atoms in the triazole ring and the sulfur atom of thiol group. Therefore, the active sites as electron donor in this ligand are approximately within the region of nitrogen and sulfur atoms. The LUMO density of this molecule in the N-N region is very high, showing that the active sites which succeed in accepting electron are from N-N region. The concentration of the electron clouds of HOMO, HOMO-2, LUMO+1 and LUMO for this ligand is mainly on S atom and the triazole ring. The HOMO energy level trough calculation with TD-DFT method is -5.753 eV, while for LUMO it is -0.395 eV, where this transference of HOMO to LUMO+1 is electron transmission from electron pairs (s) to the triazole ring of n-π* type, which has emerged in region 217 nm.

The density of the HOMO and LUMO for electron cloud of complex 1 showed that the molecular orbitals of the HOMO and LUMO were focused on the metal atom and terminal ligand of the chlorine and sulfur atoms, while the focus of the electron cloud of HOMO-1, LUMO+1 in addition to the metal atom was only on the nitrogen atoms. In the study of HOMO-2 and LUMO+2, the focus of the electron cloud on the bonded triazole rings as a bridge showed a strong electron pairing between the electron donor and the bridge (Fig. S1)

The concentration of the electron cloud of HOMO, LUMO in complex 2 is observed to be totally on sulfur atoms. On the other hand, for HOMO-2 and HOMO-1, the concentration of electron cloud is seen to be on both sulfur and nitrogen atoms. For LUMO+2 the concentration of electron cloud is seen on palladium, nitrogen, and carbon atoms.

The evaluation of electron cloud of the complexes 3 and

4 (Fig. S1) showed that in complex 3, the electron was transferred from the bridging aromatic ring of the HOMO to the LOMO one. In complex 4, however, the electronic charge density of the HOMO was observed over the sulfur atoms and the triazole aromatic ring. So, the HOMO-LUMO transition was actually the π-π* or n-π* transfer. Because the LUMO orbital of the electron cloud density was observed on d-orbital of Pd 53 and sulfur atom, the electron transfer from HOMO-2 to LUMO+1 is an indication of MMLCT transfer for the reason that in the HOMO-2 the electron cloud density is mainly delocalized over the Pd and sulfur atoms and in the LUMO+1 it was on Pd and N atoms.

Based on the investigation of Fig. S1, it can be concluded that the ligand of Hmptrz is absorbed into the surface of palladium metal from the sulfur and nitrogen site. Furthermore, the energy level of molecular orbitals in the studied complexes shows a greater stability when compared with the Hmptrz ligand. Moreover, the complexes that have electron arrangement of $d^8$, the majority of the transmissions are of metal to ligand charge transfer (MLCT) type, which is one of the factors of stability of the studied complexes.

## Natural Bond Orbital (NBO) Analysis

In this section, the NBO atomic charges were evaluated for the ligand and complexes using the Natural Population Analysis (NPA). NBO is an advanced method to study the intramolecular and intermolecular interactions and has an effective role in investigation of charge transfer or conjugative interaction system. The accumulation of the negative and positive charges on an atom indicates its prone to the electrophilic and nucleophilic attacks, respectively. The NBO analysis plays an important role in the interaction between the internal orbitals of the complexes, particularly in charge transfer. The charge distribution can provide information on the rate of the electron donation and acceptance. Using second-order perturbation theory, all the possible bonds between the filled donors and empty acceptors were studied to estimate their energetic importance and to predict the donor-acceptor (bonding-antibonding) interactions in the NBOs. The calculation was done for all the possible interactions between the occupied (donor) Lewis-type NBOs and unoccupied (acceptor) non-Lewis NBOs [57]. Such interactions lead to the loss of occupied number from the localized NBO of the idealized Lewis structure to the unoccupied non-Lewis orbitals and they do not refer to the delocalization of the natural Lewis structure. The parameters i and j are considered for each donor and acceptor, respectively. The stabilization energy $E^2$ with electron delocalization (2e stability) i→j is estimated as below [58]:

$$E^2 = q_i \frac{F^2(i,j)}{\varepsilon_J - \varepsilon_I}$$

Where, $q_i$ is the donor orbital occupancy, $\varepsilon_i$ and $\varepsilon_J$ are diagonal elements (orbital energies) and $F_{IJ}$ is off-diagonal NBO Fock matrix element.

We found that the most important interaction energy in Hmptrz (thiol) ligand was from lone-pair of the nitrogen LP (1)N4 as donor to anti-bonding orbitals π-electrons of π* (C1-N3 and C2-N5) of triazole ring as acceptor with 19.67, 16.59 kcal $mol^{-1}$ energy, respectively. In additional, this interactions is not appeared in thione form.

Other high energy interaction occur between lone-pair of LP (2)S6 to anti-bonding orbitals π* C1-N3 resulting stabilization of 10.48 kcal $mol^{-1}$as shown in Table 6.

A comparative study of the charge transfer in some bonds of the complexes is presented here. The selected NBO orbitals, its description, and occupancy are listed in Table S2.

Hmptrz has two different donor atoms, sulfur and nitrogen. According to the calculations, Pd in complex 1 bind to these ligand through the atom with the higher donor strength. In other words, Pd-nitrogen and Pd-sulfur could be formed by the donation of electron density from a lone pair (LP) orbital electrons on the nitrogen and sulfur atoms to the Pd molecular orbital (Table 7). The σ (Pd-Cl18) was formed from hybrid $spd^{1.22}$ on Pd atom (which is mixture of *s* (45.01%), *p* (0.03%), *d* (54.93%) and *f* (0.03%)) and hybrid d and $sp^{17.58}$ for Cl18 which contains 94.49% of the *p* orbital. Table S2 lists the calculated occupancies of the natural orbitals. NBO analysis showed that σ (Pd-Cl18) was strongly polarized toward the chlorine atom. Table 7 shows a comparison of second-order interaction energy ($E^2$) for 1-4 complexes, using B3LYP/TZVP and MO6 methods. The interaction strength was approximately evaluated using the second-order perturbation theory. Computing the second-

**Table 6.** Significant Donor-acceptor Interactions of Hmptrz Ligand

| Donor (i) - Acceptor (j) | | $E^2$ (kcal $mol^{-1}$) | E(j) - E(i) (a.u.) | F(i,j) (a.u.) |
|---|---|---|---|---|
| nLP(1)N4 | π*C1-N3 | 19.67 | 0.22 | 0.084 |
| nLP(1)N4 | π*C2-N5 | 16.59 | 0.23 | 0.081 |
| nLP(2)S6 | π*C1-N3 | 10.48 | 0.2 | 0.063 |
| σC1-N 3 | σ*C1-S6 | 3.46 | 0.86 | 0.069 |

**Table 7.** Significant Donor-acceptor Interactions of 1, 2, 3 and 4 Complexes at B3LYP(MO6)/TZVP

| Donor (i) | Type | Acceptor (j) | Type | $E^{(2)a}$ Kcal $mol^{-1}$ B3LYP (M06) | E( j) - E(i)[b] (a.u.) B3LYP (M06) | F(i,j)d (a.u.)[c] B3LYP (M06) |
|---|---|---|---|---|---|---|
| Complex 1 | | | | | | |
| S20 | nLP(2) | Pd17-Cl19 | σ* | 46.78(56.82) | 0.23(0.36) | 0.131(0.147) |
| N12 | nLP(1) | Pd17-Cl18 | σ* | 35.48(52.77) | 0.32(0.49) | 0.137(0.205) |
| N15 | n LP(1) | C 6-S20 | π* | 0.14(0.22) | 0.095(0.118) | 36.05(36.52) |
| N14 | nLP(1) | C 6-S20 | π* | 31.50(33.66) | 0.16(0.23) | 0.094(0.115) |
| Complex 2 | | | | | | |
| C15-N41 | π | C15-S57 | σ* | 70.57(77.07) | 0.65(0.70) | 0.274(0.281) |
| N46 | nLP(2) | C22–N45 | π* | 69.20(76.62) | 0.11(0.18) | 0.111(0.122) |
| N43 | nLP(2) | C20 –N42 | π* | 68.55(44.53) | 0.11(0.29) | 0.111(0.105) |
| N37 | nLP(2) | C6–N36 | π* | 67.61(72.73) | 0.10(0.28) | 0.108(0.115) |
| N38 | nLP(1) | O63-H64 | σ* | 15.51(27.95) | 0.71(0.85) | 0.134(0.139) |
| Complex 3 | | | | | | |
| N44 | nLP(2) | C41-N43 | π* | 73.21(79.03) | 0.11(0.18) | 0.112(0.119) |
| S46 | nLP(3) | Pd11-S12 | σ* | 52.36(62.02) | 0.28(0.34) | 0.008(0.012) |
| N22 | nLP(1) | C13-N20 | π* | 49.92(51.07) | 0.13(0.18) | 0.102(0.109) |
| N34 | nLP ( 1) | Pd11-N22 | σ* | 49.09(55.05) | 0.41(0.50) | 0.181(0.193) |
| C41-N43 | π | C36-N45 | π* | 10.40(15.41) | 0.27(0.34) | 0.074(0.081) |
| Complex 4 | | | | | | |
| N21 | nLP(2) | N11-C23 | σ* | 62.84(67.37) | 0.11(0.18) | 0.105(0.109) |
| S4 | nLP(3) | Pd2-S5 | σ* | 54.14(59.86) | 0.23(0.28) | 0.142(0.147) |
| N58 | nLP(1) | Pd1-N7 | σ* | 45.73(50.46) | 0.39(0.45) | 0.169(0.174) |
| N13 | nLP(1) | Pd 1-N10 | σ* | 40.85(49.34) | 0.39(0.44) | 0.161(0.170) |

[a]$E^{(2)}$ means energy of hyperconjugative interactions. [b]Energy difference between donor and acceptor i and j NBO orbitals. [c]F(i,j) is the Fock matrix element between i and j NBO orbitals.

order interaction energy among the studied complexes indicated that the strongest interaction of electron donor in complex 1 was related to the donation of nLP (2) S20 and acceptance of anti-bonding orbital of σ* Pd17-Cl19. The value of $E^2$ for LP(2)S20-σ* (Pd17-Cl19) is 46.78 (B3LYP/TZVP) and 56.82 (MO6) kcal $mol^{-1}$ ). On the other hand, as shown in Table S2, the nLP (2) S20 orbital had 94.67% *p*-character and 0.770e occupation (the amount included a delocalization of electron density from the occupied idealized occupancy, which had 2e).

Additionally, for complex 2 the strongest interactions were associated with the bond from π C15-N41 as donor to σ* C15-S57 antibonding orbital as acceptor (π C15-N41-σ *C15- S57), which was located on the bridge between the two dication cores of the Pd (with 70.57 (B3LYP/TZVP) and 77.07 (MO6) kcal $mol^{-1}$ energies), in fact it was an intra-molecular interaction, hyper conjugated type between σ and π leading to a stability of the molecule (Table 7).

On the Other hand, the maximum interaction energies in this complex involves the electron donating from nLP (2) N46 atom to π* (C27-N45) antibonding orbital as acceptor (with 69.20 (B3LYP/TZVP) and 76.62 (MO6) kcal $mol^{-1}$ energies) that led to a strong stability. *e.g*. nLP (2)N46-π* (C22-N45).

The NBO analysis indicated that non-conventional intramolecular hydrogen bonds involving interaction between the lone pair LP (1) N38 of the proton acceptor and anti-bond (σ* (1) O63-H64) of proton donor is characterized by a notable $E^{(2)}$ 15.51(27.95) kcal $mol^{-1}$ stabilization energy.

Examining the important interactions in complex 3, we found that the strongest donation was from LP (2) N44 to anti-bonding orbitals of π* C41-N43 with 73.21 kcal $mol^{-1}$ energy. The hybridization of the C41-N43 was sp for carbon and nitrogen atoms. On the other hand, the interaction from LP (3) S46 to antibonding σ* (Pd11-S12) with 52.36 (B3LYP/TZVP) and 62.02 (MO6) kcal $mol^{-1}$ energies and with p and $sd^{0.85}$ hybridization for Pd atom containing *s* (53.65%), *p* (0.58%), *d* (45.69%), and *f* (0.07%) created the stability in the structure of this complex (Table S2). Another reason for the stability was associated with the resonance structure between π and anti-bonding π* with 10.40 kcal $mol^{-1}$ energy, which was related to π (C41-N43) bond and π* (C36-N45). According to our investigation, the intramolecular charge transfer nLP-π*, nLP-σ* and π-π* occurs in complex 3 molecule.

One of the most important energy interactions that caused the stability in complex 4 was the transfer from the LP (1) of N21 to antibonding acceptor σ* (N11-C23). The LP (1) N21 is occupied by 0.64303e and has 99.86% *p*-character with 62.84 (67.37) kcal $mol^{-1}$ energy. On the other hand the maximum interaction energies involving the electron donations from LP (3) of S4 atom to σ* (Pd2-S5) antibonding orbital acceptor with (54.14 (59.86) kcal $mol^{-1}$) energy.

The results given in Table 7 indicated that the second-order perturbation theory analysis of fock matrix in NBO basis by the MO6 method is a little more than the B3LYP/ TZVP for all complexes.

## FT-IR Spectroscopy

Vibrational spectroscopy plays a crucial role in identifying the organic compounds functional groups to investigate the molecular conformations and reaction kinetics [59-62]. The Tables S3 and S4, the experimental vibrational frequencies of free ligand and metal complexes are compared with calculated vibrational frequencies calculated by B3LYP/TZVP method. Furthermore, the PED was evaluated, which was reported previously [63-66]. It is worthy to note that the PED explained the detailed vibrational assignments of the complex and ligand. The previous studies results [67] have suggested that the use of scaling down is necessary for the harmonic frequencies calculation in order to have better comparison with the experimental data. Therefore, in this study, the scale factor of 1.004 [68], was assigned, which seems to be adopted to the experimental results.

Our investigation of the free ligand (Hmptrz) showed that this compound consists of 12 atoms and 30 vibration modes. The selected calculated frequencies and experimental values for free Hmptrz and ethylene diamine (en) ligands are listed in Table S3.

FT IR spectra, the absorption band at 1516 $cm^{-1}$ is due to N=N stretching and also the presence of peaks around 1403-1600 $cm^{-1}$ areas is due to C=N stretching. Another recognizing method of (thione-thiol) tautomeric forms in this ligand can also be appeared of C=S band at 1216 $cm^{-1}$

for (=S) thione form and the peak in the area at 2678 $cm^{-1}$ for (-SH) thiol form.

Table S4 shows the main stretching frequencies of the studied complexes that were calculated using DFT and was demonstrated their comparison with experimental data. It is obvious that some frequencies were specific for the structure of the complex reported in a special range. Comparing the theoretical and experimental data, we found that the vibrational wavenumber in the theoretical data was more than the experimental ones because the present systems were free from anharmonicity.

It is evident that the stretching vibration of N-H aromatic ring generally appears around 3500-3220 $cm^{-1}$ [69].

The bands appeared in the FT-IR spectrum of compound 1 in the region of 3366-2933 $cm^{-1}$, are assigned to the N-H and C-H stretching vibrations in the 1-(1-($\lambda^2$-azanyl)ethyl)-4-methyl-5-($\lambda^1$-sulfanyl)-4H-1$\lambda^4$,2,4-triazole. The absorption bands at 3450-2983 $cm^{-1}$ due to the $NH_2$ stretching vibrations belong to ethylene diamine in the IR spectra of 2-4 [Fig. S3]. Moreover, the N-H stretching frequency was sharper in the Pd(II) complexes than the ligand. The PED of this modes show that they are pure stretching modes.

The FT-IR spectrum for compound 3 showed several bands within the range 3131-2927 $cm^{-1}$, which are related to C-H stretching vibration of the triazole ring and methyl group. All aromatic and aliphatic C-H modes are pure stretching modes as it is evident from PED analysis, they are almost 100%.

The investigation of the IR spectrum of the free ligand showed that, when the Hmptrz ligand coordinates to Pd(II), stretching vibrations of triazole ring are shifted to higher frequency. Therefore, when the free ligands was compared to the Pd(II) complexes, some interesting results were obtained, the stretching frequency of C=N was located around 1400-1600 $cm^{-1}$ [70]. Obviously, the nature of substituents on the N and C atoms was effective on the stretching frequencies of the C=N group. Also, C=N stretching frequency had a shift towards the higher frequency in the complexes compared to the ligand, which suggests the coordination of the ligand to the metal. The computed vibration is assigned to C=N stretching vibration at 1599 $cm^{-1}$ using B3LYP/TZVP for free ligand (which is comparable to the computed vibration of complexes 1, 2, 3 and 4) was shifted to higher frequency by 11-25 $cm^{-1}$ (Table S4). The PED for this mode indicated that this is a mixed mode. The bands observed within the range 1081-500 $cm^{-1}$ are assigned to the C=S stretching and C=S, N-N and C-N deformation vibrations. The other theoretically calculated CNC, SCN, NCN vibrations such as in-plane bending and out-of-plane bending vibrations of SCN are also in agreement with experimental data.

The band observed at 2681 $cm^{-1}$ in the IR spectrum of free Hmptrz ligand is assigned to -SH stretching vibration. A comparison between the spectra of ligand and all complexes showed that this peak disappeared for complexes 1-4. Furthermore, the absorption bands were appeared at 375 $cm^{-1}$ for 1, 315-344 $cm^{-1}$ for 2, 341 $cm^{-1}$, 189 $cm^{-1}$ for 3 and 218-323 $cm^{-1}$ for 4 are due to Pd-S vibration. In the study of complex 1, the presence of the medium peaks were in the area of (372, 321, 282 $cm^{-1}$) and (388, 361, 321 $cm^{-1}$) which were due to *cis*-square-planar structure and different distance of Pd-Cl. There are in good agreements with the experimental data. The PED of this modes show that they are pure stretching modes.

To see correlation between the calculated and experimental wavenumbers of Hmptrz ligand and complexes 1-4 correlation graphs were plotted and given in Figs. 5a-e, respectively. The relations between the calculated and experimental wavenumbers are usually linear and given by the following:

$\upsilon$Cal = 1.0284$\upsilon$exp - 30.242 for Hmptrz
$\upsilon$Cal = 0.099$\upsilon$exp + 16.72 for complex 1
$\upsilon$Cal = 0.9836 $\upsilon$exp + 16.608 for complex 2
$\upsilon$Cal = 1.0058$\upsilon$exp - 8.5373 for complex 3
$\upsilon$Cal = 0.9795$\upsilon$exp - 23.569 for complex 4

The correlation coefficients ($R^2$ values) between the calculated and experimental wavenumbers were calculated as $R^2$ = 0.9986 for Hmptrz, $R^2$ = 0.9994 for complex 1 and $R^2$ = 0.9987 for complex 2, $R^2$ = 0.9989 for complex 3, $R^2$ = 0.9991 for complex 4.

## UV-Vis Spectroscopy

The electronic absorption of the Hmptrz ligand and complexes 1, 2, 3 and 4 in DMSO at room temperature were evaluated using TD-DFT.

**Table 8.** Selected Eexperimental and Calculated (TD-DFT) Absorption Spectra of 1-4 Complexes in DMSO

| Compounds | $\lambda_{max\text{-}exp/nm\ [27]}$ | $\lambda_{max\text{-}calc/nm}$ | Molecular orbitals | $f_{calc}$ | Assignation |
|---|---|---|---|---|---|
| 1 | 231 | 361 | HOMO-1(β)-LUMO(β) | 0.947 | L←$Pd^{2+}$ |
| | 284 | 656 | HOMO-3(β)-LUMO+2(β) | 0.390 | $^1A_2g \leftarrow {}^1A_1g$ |
| | | 573 | HOMO-3(β)-LUMO(β) | 0.927 | $^1B_2g \leftarrow {}^1A_1g$ |
| | | 545 | HOMO-6(β)--LUMO(β) | 0.425 | $^1Eg \leftarrow {}^1A_1g$ |
| 2 | 259 | 251 | HOMO-6(α)-LUMO (α) | 0.386 | [π-π*] intraligand (IL) transition |
| | 325 | 325 | HOMO-7(α)-LUMO (α) | 0.366 | dσ*($Pd_2$)-π*(triazole) |
| | 423 | 456 | HOMO-8(α)-LUMO (α) | 0313 | MLCT |
| | | 489 | HOMO-12(α)-LUMO (α) | 0.207 | MMLCT |
| 3 | 262 | 261 | HOMO-2(α)-LUMO+2(α) | 0.847 | ILCT |
| | | 312 | HOMO(α)-LUMO+4(α) | 0.482 | ILCT mixed MMLCT |
| | | 382 | HOMO-6(α)-LUMO+1(α) | 0.208 | ILCT mixed MMLCT |
| | 423 | 470 | HOMO-5(α)-LUMO+1(α) | 0.206 | MLCT |
| 4 | 262 | 247 | HOMO-11(α)-LUMO(α) | 0.368 | [π-π*]intraligand(IL)transition |
| | 312 | 313 | HOMO-6(α)-LUMO(α) | 0.483 | MLCT |
| | | 338 | HOMO-5(α)-LUMO(α) | 0.795 | π-π* |
| | | 459 | HOMO-10(α)-LUMO(α) | 0.256 | MMLCT |

The TD-DFT spectral calculations have been carried out at B3LYP/def2 TZVP level of theory. Comparison between the experimental and theoretical UV-Vis spectrum is shown in Table 8. One of the diagnostic methods for (thione-thiol) tautomeric forms is the use of UV spectroscopy. The calculated TD-DFT spectrum for Hmptrz show single peak at 217 nm. We note that the absorption maximum band at 217 nm is due to the presence of the chromophoric C=S group. Figure S4 indicate that the calculated result of Hmptrz ligand show a good agreement with experimental data but it shifted to shorter wavelength compared with experimental data(~44 nm) [28].

The calculated B3LYP TD-DFT results indicated that [HOMO-1 (β) → LUMO (β)]; [HOMO-6 (α) → LUMO (α)], [HOMO-2 (α) → LUMO+2 (α)] and [HOMO-5(α)-LUMO] are the highest absorption bands, for complexes 1, 2, 3 and 4, respectively.

The complex 1 shows four absorption bands that three of them (656, 545, 361 nm) are attributed to electronic transitions of square-planar geometry Pd(II) complex and the fourth (289 nm) is attributable to metal to ligand (MLCT).

It is known that Metal-to-ligand charge-transfer (MLCT) is in general observed for transition-metal complexes with $d^8$ configurations [71].

The maximum absorption wavelength of complex 2 is 325 nm that is attributable to electron from $d$σ*($Pd_2$) HOMO to the brigading triazole ligands. The TD-DFT

calculation indicates electronic transition at 259 nm is good agreement with the experimentally measured intense band at 251 nm in DMSO.

The highest energy band for 3 is attributed to internal ligand transitions (π-π* in triazole ring) at 261 nm. Furthermore, the lowest energy band computed are assigned to admixture of an interligand π-π* transition (IL) and the MMLCT [dσ*($Pd_2$)-π*(triazole)] transition at 312 nm and 382 nm, respectively. It is notable that metal-metal-to-ligand charge transfer (MMLCT) involves a charge transfer between the filled Pd-Pd bonding orbital and a vacant, ligand-based π* molecular orbital [72].

UV-Vis spectrum of 4 in DMSO contains four bands (Fig. S4): the band exhibit at 459 nm is attributed to [*d*σ*($Pd_2$)-π*(triazole)] metal-metal to ligand charge transfer, MMLCT transitions [73]. Moreover the highest energy electronic transitions of this complex at 338 attributed to ILCT [HOMO-5-LUMO] and the transition at 312 nm and 248 nm are assigned to metal to ligand charge transfer [MLCT, HOMO-6-LUMO] and the [$\pi_{triazole}$-$\pi^*_{triazole}$] intraligand (IL) [HOMO-11-LUMO] transition, respectively.

The comparison of the theoretical and experimental data also revealed that the Hmptrz ligand tends to accept the electron from Pd(II), which is due to having an empty and low-energy π* orbital and MLCT transition. The color of the complex can also be attributed to this type of transitions. In general, the calculated B3LYP TD-DFT of all compounds are showed good agreement with the experimental results [74] (see also Table 8).

## CONCLUSIONS

In summary, we have calculated the 4-methyl-4H-1,2,4-triazole-3-thiol (Hmptrz) as ligand and four palladium(II) complexes involving one Pd(II) monomer and three $Pd^{II}$-$Pd^{II}$ dimers supported by N,S-chelating and N-S bridging. The geometry of 4-methyl-4H-1,2,4-triazole-3-thiol (Hmptrz) and palladium complexes were optimized by DFT-B3LYP method with TZVP basis set. The calculated structural parameters (bond distances and bond angles) were found to agree well with the experimental values. The quantum chemical parameters of Hmptrz and palladium complexes have calculated. In the present study, $E_{HOMO}$, $E_{LUMO}$, energy gap ($\Delta E = E_{LUMO} - E_{HOMO}$), chemical hardness η and dipole moment μ were evaluated and discussed. Our calculated results indicated that the energy gap for all complexes is smaller than the Hmptrz ligand.

The Natural bond orbital (NBO) analysis indicated that donation from the sites of electron-donor ligand to the Palladium molecular orbital was responsible for the formation of chemical bonds, hyper conjugative interactions and electron delocalization, point to the stabilization of all complexes. According to our results, NBO atomic charges analysis shows that charge transfer occur within the all molecules under investigation.

The comprehensive theoretical studies on vibrational frequencies, were performed by employing DFT-B3LYP method using TZVP. All the bands in the IR spectra have been made on the basis of the calculated potential energy distribution (PED). We then theoretically calculated and assigned the UV-Vis and electronic absorption spectra, using the state-of-the-art TD-DFT method with the B3LYP scheme which is in reasonable agreement with experiment values.

## ACKNOWLEDGEMENTS

We gratefully acknowledge the support provided by the University of Damghan, Islamic Azad University Qaemshahr and University of Farhangian.

## REFERENCES

[1] R.D. Willett, G. Pon, C. Nagy, Inorg. Chem. 40 (2001) 4342.

[2] A. Kamal, M.A. Syed, S.M. Mohammed, Expert. Opin. Ther Pat. 25 (2015) 335.

[3] a) W. Li, Q. Wu, Y. Ye, M. Luo, L. Hu, Y. Gu, F. Niu, J. Hu, Spectrochim. Acta A60 (2004) 2343. b) B. Mernari, H. Elattari, M. Triasnel, F. Bentiss, M. Langrenee, Corros. Sci. 40 (1998) 391.

[4] P. Gourdon, J.H. Andersen, K.L. Hein, M. Bublitz, B.P. Bendersen, X. Liu, L. Yatime, M. Nyblom, T.T. Nielsen, C. Olsen, J.V. Møller, P. Nissem, J.P. Morth, Growth Des. 11 (2011) 2098.

[5] P.C. Unangst, G.P. Shurum, D.T. Connor, R.D. Dyer, D.J. Schrier, J. Med. Chem. 35 (1992) 3691.

[6] V. Thottempudi, F. Forohar, D.A. Parrish, J.M. Shreeve, Angew. Chem., Int. Ed. Engl. 51 (2012) 9881.
[7] J.K. Shneine, Y.H. Alaraji, IJSR.NET. 5 (2016) 1411.
[8] J. Burschca, A. Dualeh, F. Kessler, E. Baranaoff, N. Crevey-Ha, C. Yi, M.K. Nazeeruddin, M. Grätzel, Am. Chem. Soc. 133 (2011) 18042.
[9] Y. Hau, S. Chang, D. Huang, X. Zhou, X. Zhu, J. Zhao, T. Chen, W.Y. Wong, W.K. Wong, Chem. Mater. 25 (2013) 2146.
[10] D.-Y. Huang, H. Hong-Mei, P.-F. Yao, X.-H. Qin, F.-P. Huang, Q. Yu, H.-D. Bian, Polyhedron 97 (2015) 260.
[11] M.H. Klingele, S. Brooker, Coord. Chem. Rev. 241 (2003) 119.
[12] S. Ozturk, M. Akkurt, A. Casiz, M. Koparir, M. Sekerci, F.W. Heinemann. Acta Cryst. E60 (2004) O642.
[13] D.C. Pinto, C.M. Santos, A.M. Silva, Recent Res. Dev. Heter. Chem. 37 (2007) 397.
[14] A.V. Dolzhenko, G. Pastorian, W.K. Chiu, Tetrahedron Lett. 50 (2009) 2124.
[15] S.C. Holam, B.F. Straub, New J. Org. Syn. 43 (2011) 319.
[16] R.M. Balabin, J. Chem. Phys. 131 (2009)1.
[17] I. Bertini, H.B. Gray, E.I. Steifel, J.S. Valentine, Biological Inorganic Chemistry Structure and Reactivity, University Science Books, USA, 2006
[18] F.A. Cotton, G. Wilkinson, C.A. Murillo, M. Bochmann, Advanced Inorganic Chemistry, John Wiley & Sons, New York, 1999
[19] M. Murahashi, H. Kurosawa. Coord. Chem. Rev. 231 (2002) 207.
[20] V. Amani, A.S. Delbari, A. Akbari, M.R. Poor Heravi, M. Amin, Inorg. Chem. Res. 2 (2019) 65.
[21] E. Budzisz, M. Miernicka, I.-P .Lorenz, P. Mayer, U. Krajewska, M. Rozalki, Polyhedron 28 (2009) 637.
[22] S. Nadeem, M. Bolte, S. Ahmad, T. Fazeelat, S.A. Tirmizi, M.K. Rauf, S.A. Sattar, S. Siddiq, A. Hameed, S.Z. Haider, Inorg. Chim. Acta 363 (2010) 3261.
[23] X.L. Hou, Z.M. Ge, T.M. Wang, W. Guo, J.R. Cui, T.M. Cheng, C.S. Lai, R.T. Li, Bioorg. Med. Chem. Lett. 16 (2006) 4214.
[24] J.G. Matecki, A. Maroń, Transit. Met. Chem. 36 (2011) 297.
[25] A.C. Moro, A.C. Urbaczek, E.T. De Almeida, F.R. Pavan, C.Q.F. Leite, A.V.G. Netto, A.E. Mauro, J. Coord. Chem. 65 (2012) 1434.
[26] A. Maroń, J.E. Nycz, B. Machura, J.G. Małecki, Chem. Select 4 (2016) 798.
[27] J.G. Małecki, P. Zwolin´ Ski, Polyhedron 39 (2012) 85.
[28] S. Seyfi, R. Alizadeh, M.D. Ganji, V. Amani, Polyhedron 134 (2017) 302.
[29] F. Neese, Wiley Interdiscip. Rev. Comput. Mol. Sci. 2 (2012) 73.
[30] H. Haberland, Ed. W., John Whiey & Sons, 1999, p. 181.
[31] F. Weigend, R. Ahlrichs, Chem. Phys. 7 (2005) 3297.
[32] A.D. Becke. J. Chem. Phys. 98 (1993) 5648.
[33] C. Lee, W. Yang, R.G. Parr, Phys. Rev. B 37 (1988) 785.
[34] D. Andrae, U. Haeussermann, M. Dolg, H. Stoll, H. Preuss, Theor. Chem. Acc. 77 (1990) 123.
[35] U. Haeussermann, M. Dolg, H. Stoll, H. Preuss, Mol. Phys. 78 (1993) 1211.
[36] E.D. Glendening, A.E. Reed, J.E. Carpenter, F. Weinhold, J. Am. Chem. Soc. 120 (1998) 12051.
[37] a) Y. Zhao, D.G. Truhlar, J. Chem. Phys. 125 (2006) 1. b) Y. Zhao, D.G. Truhlar, Theor. Chem. Acc. 120 (2008) 215.
[38] A. Klamt, G. Schüürmann, J. Chem. Soc. Perkin Trans. 2 (1993) 799.
[39] M.E. Casida, J. Theor. Comput. Chem. 4 (1996) 391.
[40] M.H. Jamróz, Vibrational Energy Distribution Analysis, VEDA 4, 2004.
[41] M.H. Jamróz, Spectrochim. Acta Mol. Biomol. Spectrosc. 114 (10) (2013) 220.
[42] V. Krishnakumar, R.J. Xavier, Spectrochimica Acta Part A 60 (2004) 709.
[43] H.-Y. Wang, P.-S. Zhao, R.-Q. Li, S.-M. Zhou, Molecules 14 (2009) 608.
[44] J. Luo, J.R. Khusnutdinova, N.P. Rath, L.M. Mirica, Chem. Commun. 48 (2012) 1532.
[45] B.-H. Xia, C.-M., Z.-Y. Zhou, Chem. Eur. J. 9 (2003) 3055.
[46] J.E. Bercaw, A.C. Durrell, H.B. Gray, J.C. Green, N.

Hazari, J.A. Labinger, J.R. Winkler.Inorg, Chem. 49 (2010) 1801.

[47] a) K.R. Mann, J.G. Gordon, H.B. Gray, J. Am. Chem. Soc. 97 (1975) 3553.(b) R.G. Parr, R.G. Pearson, J. Am. Chem. Soc. 105 (1983) 7512.

[48] G. Heimel, L. Romanerb, E. Zojerc, J.-L. Brédasd, Organic Optoelectronics and Photonics III, Proc. of SPIE, 6999 (2008) 699919. b) R.D. Vargas-Sánchez, A.M. Mendoza-Wilson, R.R. Balandrán-Quintana, G.R. Torrescano-Urrutia, A. Sánchez-Escalante, Comput. Theor. Chem. 1058 (2015) 21.

[49] S. Baishya, R.C. Deka, Comput. Theor. Chem. 1002 (2012) 1.

[50] J. Sam, J. Abraham, Ind. Eng. Chem. Res. 51 (2012) 16633.

[51] H.O. Kalinowski, S. Berger, S. Braun, Carbon-13 NMR Spectroscopy, John Wiley and Sons, Chichester, 1988.

[52] I. Fleming, Frontier Orbitals and Organic Chemical Reactions, Wiley, London, 1976.

[53] M. Karelson, V.S. Lobanov, R. Katritzky, Chem. Rev. 96 (1996) 1027.

[54] K.F. Khaled, K. Babic´-samaradzija, N. Hackerman, Appl. Surf. Sci. 240 (2005) 327.

[55] D.G. Truhlar, J. Chem. Phys. 82 (1985) 2418.

[56] R.P. Gangadharan, S.S. Krishnan, Acta Physica Polonica A 125 (2014) 18.

[57] N. Günaya, Ö. Tamerb, D. Kuzalicc, D. Avci, Y. Atalayb, Acta Physica Polonica A 127 (2015) 701.

[58] K. Bahgat, S. Fraihat, Spectrochim. Acta Mol. Biomol. Spectrosc. 135 (2015) 1145.

[59] D.M. Samiei Paqhaleh, A.A. Aminjanov, V. Amani, A. Morsali, J. Inorg. Organomet. Polym. Mater. 24 (2014) 340.

[60] Y.L. Wang, N. Zhang, Q.Y. Liu, Z.M. Shan, R. Cao, M.S. Wang, J.J. Luo, E.L. Yang, Cryst. Growth Des. 11 (2011) 130.

[61] Y.L. Jiang, Y.L. Wang, J.X. Lin, Q.Y. Liu, Z.H. Lu, N. Zhang, J.J. Wei, L.Q. Li, Cryst. Eng. Comm. 13 (2011) 1697.

[62] J.P. Jesson, H.W. Thompson, Spectrochim. Acta 13 (1958) 217.

[63] J. Jolley, W.I. Cross, R.G. Pritchard, Ch.A. McAuliffe, K.B. Nolan, Inorg. Chim. Acta 315 (2001) 36.

[64] J. Sam, J. Abraham, Eng. Chem. Res. 51 (2012) 16633.

[65] D.J. Charboneau, N.A. Piro, W. Scott Kassel, T.J. Dudley, J. Paul. Polyhedron 91 (2015) 18.

[66] Ch. Gabbiani, A. Casini, L. Messori, A. Guerri, M.A. Cinellu, M. Corsini, C. Rosani, P. Zanello, M. Arca, Inorg. Chem. 47 (2008) 2368.

[67] S. Sangilipandi, R. Nagarajaprakash, D. Sutradhar, W. Kaminsky, A.K. Chandra, K.M. Rao, Inorg. Chim. Acta 437 (2015) 177.

[68] G. Zhang, Ch.B. Musgrave, J. Phys. Chem. A 111 (2007) 1554.

[69] R.N. Singh, R.K. Amit Kumar, T. Spectrochim. Acta, Part A 112 (2013) 182.

[70] M.M. El-Nahass, M.A. Kamel, A.F. El-deeb, A.A. Atta, S.Y. Huthaily, Spectrochim. Acta, Part A 79 (2011) 443.

[71] R.C. Evans, P. Douglas, C.J. Winscom, Coord. Chem. Rev. 250 (2006) 2093.

[72] S.-W. Lai, C.-M. Che, Top. Curr. Chem. 241 (2004) 27.

[73] J.-C. Shi, T.-B. Wen, Y. Zheng, S.-J. Zhong, D.-X. Wu, Q.-T. Liu, B.S. Kang, B.-M. Wu, T.C.W. Mak, Polyhedron 16 (1997) 369.

[74] P.T. Chou, Y. Chi, Chem. Eur. J. 13 (2007) 380.